EUSAR 2021 . ISBN 978-3-8007-5457-1 / ISSN 2197-4403 . ©VDE VERLAG GMBH . Berlin . Offenbach

A Compensation Method Based on Electromagnetic Vortex Synthetic Aperture Radar Imaging

Gaofeng Shu[a,b], Wentao Wang[a], and Heng Zhang[a]
[a]Department of Space Microwave Remote Sensing Systems, Aerospace Information Research Institute, Chinese Academy of Sciences, Beijing 100094, China
[b]School of Electronics, Electrical and Communication Engineering, University of Chinese Academy of Sciences, Beijing 100049, China

Abstract

Electromagnetic (EM) waves carrying orbital angular momentum (OAM) has a spiral phase wavefront, which can be applied to radar as well as wireless communication. It is reported that synthetic aperture radar (SAR) imaging based on vortex EM waves can achieve azimuth high resolution. Meanwhile, point targets defocus due to the two-dimensional space-variant distribution of intensity and phase of vortex beams. In this paper, the distortion of targets caused by vortex beams is discussed and a compensation method to solve the distortion in vortex SAR imaging is proposed. The simulation results show the effectiveness of the proposed algorithm.

1 Introduction

The application of vortex beams, light beams or electromagnetic (EM) waves carrying orbital angular momentum (OAM), is rapidly developed during the past few decades[1, 2]. Vortex EM waves have a potential to provide new degrees of freedom[3, 4] due to its spiral phase wavefront, which is described by the spatial azimuthal phase term $\exp(\mathrm{j}l\phi)$ where l is an integer and ϕ refers to the azimuthal angle. The beams with different values of l, i.e., different OAM modes, are mutually orthogonal to each other and can thus theoretically contain an infinite number of eigenstates[5], which has quickly gained widespread attention in wireless communication fields[6, 7].

There are appreciable prospects that the application of OAM beams to radar imaging[8, 9] or target detection[10, 11] besides its application to wireless communication. When targets are illuminated by OAM beams, the reflected EM waves carry much richer information, such as the azimuth angle along the beam axis and the oblique scattering of an object, due to the helical wavefronts of the OAM modes. The azimuth angle profile of the targets can be obtained via spectral estimation method, such as fast Fourier transform (FFT) method or multiple signal classification (MUSIC) method. The rotational frequency shift of a light beam carrying OAM has been observed and measured[12, 13], hence a spinning object can be detected by using vortex beams[10, 14].

Synthetic aperture radar (SAR) is an advanced earth observation radar that has the capability of high-resolution imaging, environmental monitoring, resource mapping, and moving targets detection and is independent of weather conditions and sunlight illumination[15]. The research of vortex EM waves in radio communication and radar fields have paved the way for its application in SAR imaging. For example, a novel three dimensional SAR imaging method based on vortex EM wave is proposed, but the third dimension, i.e., the azimuth angle, is also obtained via spectral estimation method[16]. Recently, Fang *et al.* established a vortex SAR model and presented a point target simulation. It is shown that the point target will not focus unless an extra amplitude correction is carried out[17, 18]. Furthermore, a phase compensation is also essential from the results of a vehicle-borne experiment[19]. However, all of the literatures neither studied the difference between vortex SAR images and traditional SAR images, nor did they give a exact solution to the point target focusing problem. In this paper, we focus on the distortion of the targets caused by amplitude and phase modulation in vortex SAR, and a modified compensation algorithm to focus the targets.

This paper is organized as follows. In section II, a more precise vortex SAR echo model is built. Then the proposed compensation algorithm to solve the distortion problem is introduced in section III. In section IV, point targets processed by the traditional and proposed algorithm are presented and some comparisons between them are made. Conclusions are drawn in Section V.

2 Signal Model

2.1 Geometry Model

We consider a general geometry of an airborne SAR data acquisition, as shown in Fig. 1. The radar platform carrying an antenna flies along the y-axis at a constant speed of V_r and the altitude of the platform is H with respect to the ground (in most cases, the Earth). The vortex beams are generated by a uniform circular array (UCA), an antenna that can generate conveniently the OAM beams in radio domain[2]. A coordinate system (uvw) with the ori-

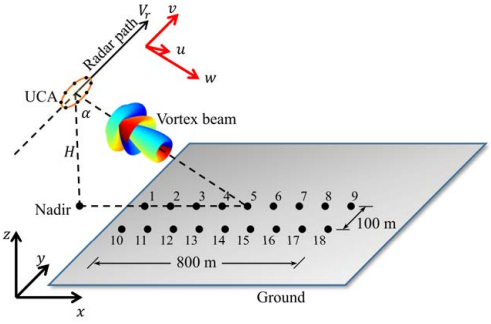

Figure 1 A simplest vortex SAR data acquisition geometry. The black numbered points placed on the ground represent point targets for simulations.

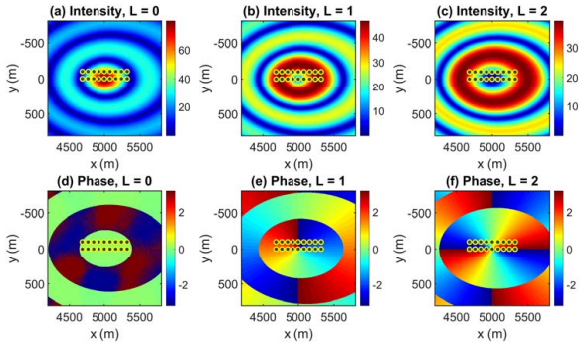

Figure 2 The intensity (top row) and phase (bottom row) distribution of the radiation field of the UCA antenna on the ground, which represents $l = 0, 1$, and 2 from left to right panel. The filled circles represent point targets on the ground.

gin at the UCA antenna phase center (APC) and the v-axis coincident with the y-axis is assumed. For a simply broadside stripmap mode, the beam axis is along the w-axis and the tilt angle with respect to nadir is denoted by α, i.e., vw plane is the slant range plane of the beam center.

2.2 Antenna Pattern of the OAM Beams

It is well known that an electromagnetic (EM) system can radiate linear momentum and angular momentum into far zone. For any EM wave with an electric field $\boldsymbol{E}$ and magnetic field $\boldsymbol{B}$, the angular momentum of the EM field is expressed as [20]

$$\boldsymbol{J} = \int \varepsilon_0 \boldsymbol{r} \times (\boldsymbol{E} \times \boldsymbol{B}) \, \mathrm{d}^3 r \tag{1}$$

where ε_0 is the permittivity of the media. However, the angular momentum can be decomposed into OAM and spin angular momentum (SAM), i.e.,

$$\boldsymbol{J} = \boldsymbol{J}_s + \boldsymbol{J}_o \tag{2}$$

where

$$\boldsymbol{J}_s = \varepsilon_0 \int \boldsymbol{E} \times \boldsymbol{A} \, \mathrm{d}^3 r \tag{3}$$

$$\boldsymbol{J}_o = \varepsilon_0 \int \boldsymbol{E}^* (\boldsymbol{r} \times \boldsymbol{\nabla}) \cdot \boldsymbol{A} d^3 r \tag{4}$$

where $\boldsymbol{A}$ is the vector potential, $\boldsymbol{\nabla} = \hat{\boldsymbol{x}} \frac{\partial}{\partial x} + \hat{\boldsymbol{y}} \frac{\partial}{\partial y} + \hat{\boldsymbol{z}} \frac{\partial}{\partial z}$ is the differential operator on three-dimensional Euclidean space in Cartesian coordinates $\{x, y, z\}$, and $(\cdot)^*$ denotes the conjugation. It is reported that $\boldsymbol{J}_s$ depends only on the local polarization structure and $\boldsymbol{J}_o$ depends on the gradient of the fields [2]. In other words, OAM is an extrinsic property with respect to the space vector.

In the uvw coordinate system, the array factor of the UCA antenna is expressed as follows[21] if the number of antenna elements N is sufficiently large

$$F(\theta, \phi, l) = J_l(ka \sin\theta) \exp(\mathrm{j} l \phi), \tag{5}$$

where

- θ angle of the pointing direction with respect to the w-axis;
- ϕ polar angle of the projection of the pointing direction on the uv plane;
- l an integer that indicates the OAM modes;
- $J_l(\cdot)$ Bessel functions of the first kind;
- j imaginary unit, i.e., $\mathrm{j} = \sqrt{-1}$;
- k wavenumber, equals $2\pi/\lambda$, being λ the wavelength of the vortex EM wave;
- a radius of the UCA antenna.

According to the peculiar phase properties of the vortex waves, the vortex beam ($l \neq 0$) has a singularity along the beam axis, and the main lobe diffuses outward as the distance increases.

In xyz coordinate system, assuming that the position of the platform at a particular time is $(0, y, H)$ and a hypothetical point target is located at $P(x_n, y_n, 0)$ on the ground, then we can obtain the slant range $r_n = \sqrt{x_n^2 + (y_n - y)^2 + H^2}$ and the minimum ground range of the beam center $x_c = H/\tan\alpha$. According to the geometry, we can deduce precisely the target angular boresight from the platform as following

$$\begin{aligned} \theta_n &= \arccos\left[\frac{\sqrt{x_n^2 + H^2}}{r_n} \cdot \cos(\alpha - \alpha_n)\right] \\ \phi_n &= \arctan\left[\frac{y_n - y}{(x_c - x_n)\cos\alpha}\right], \end{aligned} \tag{6}$$

where $\alpha_n = \arctan(x_n/H)$. It is well known that $f(x) = \arctan(x)$ is an odd function, which causes the sidelobe of a target response asymmetrical.

Fig. 2 shows the intensity and phase distribution of the radiation field of the UCA antenna on the ground. For $l \neq 0$, the greater l is, the wider null becomes in the center of the amplitude pattern and the larger phase gradient along a circle around the beam axis. Along the direction of the radar path, the intensity and phase history of a point vary with each ground range as well as each range cell.

2.3 Vortex SAR Echo Signal

Let the UCA antenna transmit the following linear frequency modulated (LFM, chirp) pulse

$$p(t) = \exp(\mathrm{j}\omega t) \exp\left(\mathrm{j}\pi K_r t^2\right) \mathrm{rect}\left(\frac{t}{T_p}\right), \quad (7)$$

where

t	the fast time variable;
$\omega = kc$	the angular carrier frequency, where c is the wave propagation speed;
T_p	pulse duration;
$K_r = B_r/T_p$	the chirp rate, being B_r the transmitted signal bandwidth;
$\mathrm{rect}(t)$	the rectangular window function, where $\mathrm{rect}(t) = 1$ if $\lvert t\rvert \leqslant 1$, and $\mathrm{rect}(t) = 0$ otherwise.

For the traditional stripmap SAR mode, the baseband echo signal from a point P can be represented by the complex signal[22]

$$s_0(t,\eta) = \sigma_n \,\mathrm{rect}\left(\frac{t - 2r_n/c}{T_p}\right) \exp\left[\mathrm{j}\pi K_r \left(t - 2r_n/c\right)^2\right] \times \mathrm{rect}\left(\eta - \eta_c\right) \exp\left(-\mathrm{j}4\pi r_n/\lambda\right), \quad (8)$$

where σ_n is the reflectivity of the target, η and η_c is the slow time variable and the crossing time of the beam center. As the platform moves, the strength of azimuth signal varies with the azimuth beam pattern. Because of the round trip of the radar energy, the vortex SAR echo signal can be modified from (8)

$$\begin{aligned} s(r,y,l) &= \sigma_n \,\mathrm{rect}\left(\frac{r - 2r_n}{cT_p}\right) \exp\left[\mathrm{j}\pi \frac{K_r}{c^2}\left(r - 2r_n\right)^2\right] \\ &\quad \times F^2(\theta_n, \phi_n, l) \exp\left(-\mathrm{j}2kr_n\right) \\ &= \sigma_n b\left(r - 2r_n\right) a\left(x_n, y_n - y, l\right), \end{aligned} \quad (9)$$

where

$$b\left(r\right) = \mathrm{rect}\left(\frac{r}{cT_p}\right) \exp\left[\mathrm{j}\pi \frac{K_r}{c^2} r^2\right] \quad (10a)$$

$$a\left(x_n, y_n - y, l\right) = F^2(\theta_n, \phi_n, l) \exp\left(-\mathrm{j}2kr_n\right) \quad (10b)$$

are the vortex SAR echo signal in the range and the azimuth direction, respectively.

The range signal $b\left(r - 2r_n\right)$ of the vortex SAR is the same as that of the traditional SAR. However, the azimuth signal contains an envelope of a Bessel function of the first kind and an extra phase term, which are both caused by the pattern of the UCA antenna, as can be seen in Fig. 2. As a result, the targets fail to focus when a traditional algorithm is used. A modified approach based on backprojection (BP) algorithm to focus the vortex SAR data is introduced in the next section.

3 Compensation Algorithm

As described in the previous section, we will focus on the azimuth signal because the range signal is the same as that of the traditional SAR echo. The azimuth signal focusing is the main step in the vortex SAR data processing. It can be seen that the azimuth signal (10b) in the vortex SAR echo varies with OAM modes and boresight, actually as well as the ground and the azimuth range. The amplitude and phase modulation of the two-dimensional space-variant makes it difficult to focus on vortex SAR targets.

As a time domain algorithm, the backprojection (BP) algorithm is considered to be the most convenient method to solve the vortex SAR focusing problem, as it can be applied to almost every SAR configuration[23]. The main steps of a basic BP algorithm is shown in Fig. 3. For the vortex SAR imaging, all of the steps are the same as the basic BP algorithm except the vortex (amplitude and phase) compensation step in the filled box.

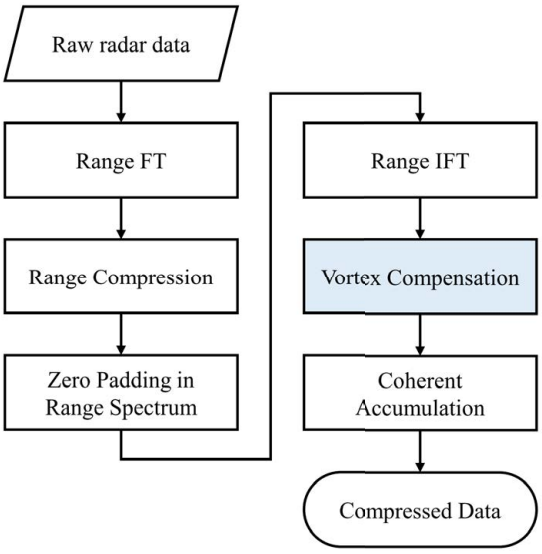

Figure 3 The functional block diagram of a modified BP algorithm.

According to (10b), the phase multiplication is

$$\tilde{h}(x_n, y_n - y, l) = \exp\left(-\mathrm{j}2l\phi_n\right) \exp\left(\mathrm{j}2kr_n\right) \quad (11)$$

instead of $\exp\left(\mathrm{j}2kr_n\right)$ in the traditional SAR system. In the meantime, the envelope of the antenna pattern can be also compensated and therefore the compensation function is given by

$$h(x_n, y_n - y, l) = \tilde{h}(x_n, y_n - y, l)/J_l^2(ka\sin\theta_n), \quad (12)$$

which can be called as the vortex compensation function. After multiplying (12) and performing the rest of the algorithm, the echoes becomes a focused image. It is noteworthy that the envelope compensation cannot improve the signal-to-noise ratio (SNR) in the presence of additive noise. In fact, SNR significantly decreases when the envelope profile has a null. This issue need to be further discussion in the future.

4 Simulation Results and Discussion

To verify the ability of the proposed compensation algorithm for focusing the ideal vortex SAR raw data, a simu-

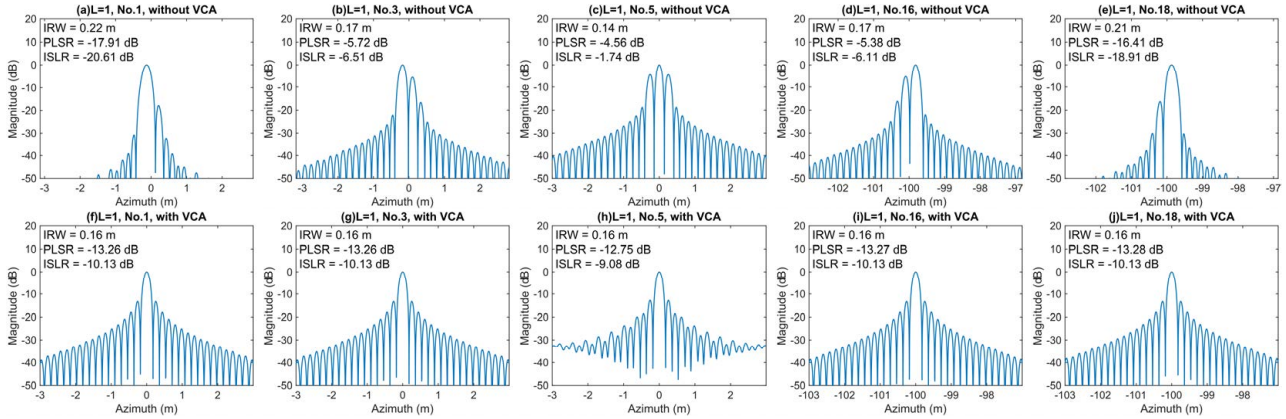

Figure 4 The azimuth profiles of the targets 1, 3, 5, 16, and 18. (a)-(f) Without the vortex compensation algorithm (VCA); (f)-(j) With the VCA. The OAM mode transmitting is $l = 1$.

Table 1 The Simulation Parameters for an Airborne Vortex SAR

Simulation parameters	Values
Carrier frequency	$f_c = 9.6$ GHz
Range bandwidth	$B_r = 600$ MHz
UCA's radius	$a = 0.32$ m
Aircraft altitude	$H = 5000$ m
Velocity along the track	$V_r = 120$ m/s
Angle between beam axis and nadir	$\alpha = 45°$
Squint angle of beam axis	$\theta_{\text{sq}} = 0$
Targets' x coordinates on ground	$x \in x_c \pm 400$ m
Targets' y coordinates on ground	$y \in [-100, 0]$ m

lation using the airborne SAR parameters given in Table. 1 is performed. The point targets are symmetrically set on the both sides of the beam center on the ground and the spacing of the adjacent targets is 100 m in the azimuth and 80 m in the range. The targets' layout is show in Fig. 1.

The azimuth profiles of targets 1, 3, 5, 16, and 18 are shown in Fig. 4a-e. It can be seen that the azimuth profiles of targets are defocused under the general BP algorithm. The amplitude modulation rises the sidelobes, and the phase modulation causes the sidelobes asymmetrical in detail as mentioned previously. This is the reason why the image quality is degraded in [17] and [19]. On the other hand, the targets focus performance deteriorates with increasing OAM mode because of drastically varying amplitude and phase history.

The simulated azimuth results were processed by using the proposed algorithm described in the previous section, and the results are shown in Fig. 4f-j. Except for the center point target, the other targets are well focused. The peak sidelobe ratio (PSLR) deviates from the theoretical value of -13.26 dB by less than 0.02 dB, and the integrated sidelobe ratio (ISLR) is within 0.13 dB from the expected value of -10.00 dB. The impulse response width (IRW) is the same of one particular OAM mode and agrees with the azimuth resolution $0.886\frac{\lambda}{2\theta_{\text{bw}}}$ calculated by the beam width and wavelength.

However, the targets near the beam center such as No. 5 result not well. The PSLR and ISLR are higher than the theoretical values and the attenuation of sidelobes is not so steep as the other targets. This is because there is a null in the center of the amplitude history in the azimuth direction. Theoretically, a null center need an infinite value to compensate. In practical, a small enough value such as 1×10^{-7} with respect to the maximum amplitude is regarded as null instead of zero.

5 Conclusion

In SAR imaging technology, the modulation of amplitude and phase of the vortex pattern causes the sidelobes of point targets to rise and be asymmetrical, respectively. A compensation algorithm to focus targets is proposed. By using the proposed algorithm, except for points near the beam center, the azimuth profiles of the targets are well focused compared with a standard sinc-like result. Future works include focusing points near the beam center, and applying the proposed algorithm to a real airborne data.

6 Literature

[1] Allen, L.: Beijersbergen, M. W.: Spreeuw, R. J. C.: Woerdman, J. P.: Orbital angular momentum of light and the transformation of Laguerre-Gaussian laser modes, Phys. Rev. A. Vol. 45, No. 11, Jun.1992, pp. 8185–8189

[2] Thidé, B.: Then, H.: Sjöholm, J.: Palmer, K.: Bergman, J.: Carozzi, T. D.: Istomin, Ya. N.: Ibragimov, N. H.: Khamitova, R.: Utilization of Photon Orbital Angular Momentum in the Low-Frequency Radio Domain, Phys. Rev. Lett.. Vol. 99, No. 8, Aug. 2007, pp. 087701

[3] Cano, E.: Allen, B.: Bai, Q.: Tennant, A.: Generation and detection of OAM signals for radio communications, 2014 Loughborough Antennas and Propagation Conference (LAPC). Nov. 2014, pp. 637-640

[4] Nguyen, D. K.: Sokoloff, J.: Pascal, O.: Chabory, A.: Palacin, B.: Capet, N.: Local Estimation of Orbital and Spin Angular Momentum Mode Numbers, IEEE

Antennas and Wireless Propagation Letters. Vol. 16, 2017, pp. 50-53

[5] Cheng, L.: Hong, W.: Hao, Z.: Generation of Electromagnetic Waves with Arbitrary Orbital Angular Momentum Modes, Scientific Reports. Vol. 4, No. 1, Apr. 2014, pp. 4814

[6] Tamburini, F.: Mari, E.: Sponselli, A.: Thidé, B.: Bianchini, A.: Romanato, F.: Encoding many channels on the same frequency through radio vorticity: first experimental test, New Journal of Physics. Vol. 14, No. 3, 2012, pp. 033001

[7] Yan, Y.: Xie, G.: Lavery, M. P. J.: Huang, H.: Ahmed, N.: Bao, C.: Ren, Y.: Cao, Y.: Li, L.: Zhao, Z.: High-capacity millimetre-wave communications with orbital angular momentum multiplexing, Nature Communications. Vol. 5, Sep. 2014, pp. 4876–4876

[8] Liu, K.: Cheng, Y.: Li, X.: Wang, H.: Qin, Y.: Jiang, Y.: Study on the theory and method of vortex-electromagnetic-wave-based radar imaging, IET Microwaves, Antennas & Propagation. Vol. 10, No. 9, Jun. 2016, pp. 961-968(7)

[9] Liu, K.: Li, X.: Gao, Y.: Cheng, Y.: Wang, H.: Qin, Y.: Qin, Y.: High-Resolution Electromagnetic Vortex Imaging Based on Sparse Bayesian Learning, IEEE Sensors Journal. Vol. 17, No. 21, Nov. 2017, pp. 6918-6927

[10] Lavery, M. P. J.: Speirits, F. C.: Barnett, S. M.: Padgett, M. J.: Detection of a Spinning Object Using Light's Orbital Angular Momentum, Science. Vol. 341, No. 6145, 2013, pp. 537–540

[11] Lin, M.: Gao, Y.: Liu, P.: Liu, J.: Super-resolution orbital angular momentum based radar targets detection, Electronics Letters. Vol. 52, No. 13, Jun. 2016, pp. 1168-1170

[12] Courtial, J.: Dholakia, K.: Robertson, D. A.: Allen, L.: Padgett, M. J.: Measurement of the Rotational Frequency Shift Imparted to a Rotating Light Beam Possessing Orbital Angular Momentum, Phys. Rev. Lett.. Vol. 80, No. 15, Apr. 1998, pp. 3217–3219

[13] Courtial, J.: Robertson, D. A.: Dholakia, K.: Allen, L.: Padgett, M. J.: Rotational Frequency Shift of a Light Beam, Phys. Rev. Lett.. Vol. 81, No. 22, Nov. 1998, pp. 4828–4830

[14] Liu, K.: Cheng, Y.: Li, X.: Wang, H.: Qin, Y.: Liu, K.: Gao, Y.: Spinning target detection using OAM-based radar, 2017 International Workshop on Electromagnetics: Applications and Student Innovation Competition. May. 2017, pp. 29-30

[15] Deng, Y.: Zhao, F.: Wang, Yu: Brief Analysis on the Development and Application of Spaceborne SAR, Journal of Radars. Vol. 1, No. 1, 2012, pp. 1

[16] Yang, T.: Li, S.: Xu, O.: Li, W.: Wang, Y.: Three dimensional SAR imaging based on vortex electromagnetic waves, Remote Sensing Letters. Vol. 9, No. 4, 2018, pp. 343-352

[17] Fang, Y.: Chen, J.: Wang, P.: Li, W.: Men, Z.: Ma, B.: Han, B.: A novel SAR imaging method based on electromagnetic vortex with orbital-angular-momentum, 2017 IEEE International Geoscience and Remote Sensing Symposium (IGARSS). Jul. 2017, pp. 1638-1641

[18] Fang, Y.: Chen, J.: Wang, P.: Men, Z.: Zhou, X.: Hu, K.: A novel imaging formation of electromagnetic vortex SAR with time-variant orbital-angular-momentum, 2018 IEEE International Geoscience and Remote Sensing Symposium (IGARSS). Jul. 2018, pp. 577-580

[19] Bu, X.: Zhang, Z.: Chen, L.: Liang, X.: Tang, H.: Wang, X.: Implementation of Vortex Electromagnetic Waves High-Resolution Synthetic Aperture Radar Imaging, IEEE Antennas and Wireless Propagation Letters. Vol. 17, No. 5, May. 2018, pp. 764-767

[20] Barnett, S.M.: Zambrini, R.: Orbital Angular Momentum of Light, In: Kolobov M.I. (eds) Quantum Imaging. Springer, New York, NY, 2007, pp. 277-311

[21] Mohammadi, S. M.: Daldorff, L. K. S.: Bergman, J. E. S.: Karlsson, R. L.: Thidé, B.: Forozesh, K.: Carozzi, T. D.: Isham, B.: Orbital Angular Momentum in Radio—A System Study, IEEE Transactions on Antennas and Propagation. Vol. 58, No. 2, Feb. 2010, pp. 565-572

[22] Cumming, I. G.: Wong, F. H.: Digital Processing of Synthetic Aperture Radar Data, Artech House Publishers, 2005

[23] Zhang, H.: Tang, J.: Wang, R.: Deng, Y.: Wang, W.: Li, N.: An Accelerated Backprojection Algorithm for Monostatic and Bistatic SAR Processing, Remote Sensing. Vol. 10, No. 1, 2018